

# NUMERICAL METHOD TO DETERMINE STRUCTURAL ELEMENT REDUCED STIFFNESS FOR DESIRED COMPOSITE WING STRUCTURES CONFIGURATIONS

Sebastian Stammel<sup>1</sup> & Chiara Bisagni<sup>1</sup>

<sup>1</sup>Politecnico di Milano, Department of Aerospace Science and Technology

#### **Abstract**

This study presents a numerical analysis on the prebuckling, postbuckling and reduced torsional stiffness as well as deformation of a simplified composite wing-box experiencing torsion. Multiple lay-up orientations and variations in the number of plies of the wing-box are investigated using eigenvalue and dynamic implicit analyses. Results show a high sensitivity of the lay-up orientation on the prebuckling and reduced torsional stiffness. A variation in the number of plies influences the postbuckling torsional stiffness as well as the deformation distribution of the wing-box. The outlook shows how these results will be used for a new methodology under investigation for the design of passively morphing aerospace structures in future.

Keywords: Stiffness; Buckling; Wing-Box; Numerical analysis

## 1. Introduction

Shape adaptivity for aerospace structures offers the potential to design structures working in multiple operational conditions [1, 2]. This capability allows optimal characteristics during each operational mission stage, reduces the structural weight, and improves efficiency. Researchers commonly realize shape adaptivity using active conventional actuators [3] and smart-actuators [4, 5] and passive design concepts [6, 7]. The latter concept utilized modified material properties and structural geometry to realize the desired shape transformation. In this context, elastic instabilities like buckling are explored to provide large deformation potential to enable the shape adaptivity of structures [8]. The non-linear postbuckling response of a wing-box structure was used for stiffness and shape changes and the adaptivity was controlled by restraining the out-of-plane buckling [9]. In contrast, large deformations and the inability to withstand loads have been considered for a long time with buckling. However recent work shows and demonstrates the capability of buckled composite stiffened panels to carry loads [10, 11].

For future use of buckling for passive shape adaptivity, the knowledge of material and geometrical influences on the buckling and stiffness behavior of aerospace structures is essential. A targeted buckling deformation of the test ribbon is achieved by manufacturing a specific pre-defined thickness variation into it [12]. This targeted deformation can be also changed by tuning the thickness ratio or the length of the thickness variation. Apart from a thickness variation, the ply orientation variation within a composite also influences the buckling and stiffness behavior. This stiffness tuning with a piecewise variable ply orientation in a composite panel creates multiple target shapes for a panel under loading [13, 14].

This study consists of a numerical investigation of a simplified composite wing-box experiencing torsion load. Numerical analyses are conducted to study the influences of orientation and the number of plies on the stiffnesses and deformation of the wing-box. Finite-element analyses are performed with *ABAQUS* [15] to investigate the sensitivities of buckling rotation and moment as well as prebuckling, postbuckling, and reduced torsional stiffness. The results will help to understand the impact of

composite material characteristics on the torsional stiffness of a wing-box for the future development of a methodology for the design of a passively morphing wing-box.

The wing-box model used for the numerical analysis is presented in section 2. The numerical analyses are outlined in section 3. Afterward, the results of the numerical analyses are shown in section 4. The conclusions of this investigation are shown in section 5. The idea of the new design methodology in development using the results of this investigation is presented in section 6.

# 2. Simplified Wing-Box sturcture

The investigation is conducted with a simplified wing-box. The simplified wing-box for the investigation is shown in figure 1.

The wing-box consists of the front and rear spar as well as the top and bottom skin. Ribs are not considered for the simplified model. The wing-box has a length l of 2400 mm, a width b of 500 mm, and a height h of 200 mm. The wing-box is divided along the x-axis into 8 equal segments, each segment  $l_{seg}$  300 mm long. The connection to the aircraft fuselage is represented by the root frame of the wing-box. The root frame is constrained regarding rotation and displacement in any direction. The tip frame represents the connection to the wing tip area and rotation as well as displacement is allowed. The aerodynamical loading of the wing-box is modeled as a torsional rotation at the centerpoint of the tip frame of the wing-box. An imposed wing-box rotation of  $\theta_x = 10^\circ$  around the x-axis is chosen as torsional rotation.

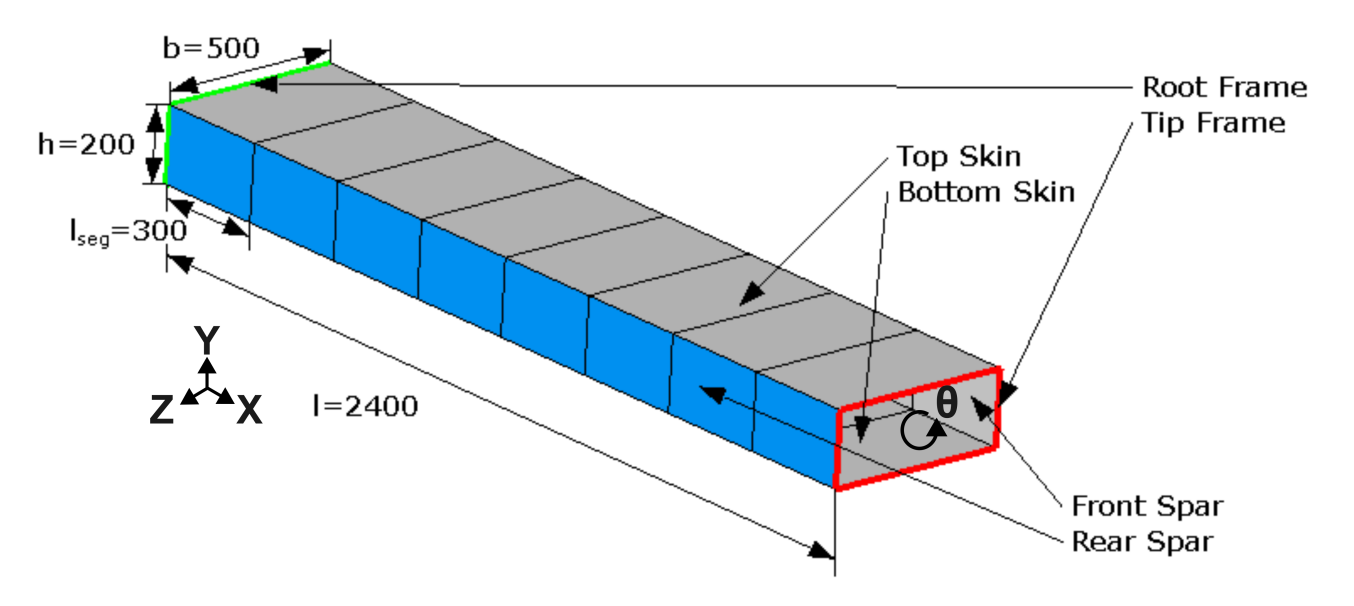


Figure 1 – Sketch of simplified wing-box. Dimensions in [mm].

The wing-box is built out of *IM7/8552* composite material containing carbon fibers and a thermoset resin. Table 1 reports material characteristics of the composite material.

$E_{11}[MPa]$	$E_{22}[MPa]$	$G_{12}[MPa]$	<b>v</b> [-]	$\rho\left[\frac{kg}{m^3}\right]$	$t_{ply}[mm]$
150000	9080	5290	0.32	1570	0.125

Table 1 – Unidirectional *IM7/8552* composite ply properties [16].

For the numerical study, the number of plies and the orientation of the composite for the wing-box are varied. Two different orientations and three different numbers of plies are used resulting in six different configurations of the wing-box. Table 2 contains all configurations for the study.

The first configuration quasi-isotropic-baseline uses a quasi-isotropic lay-up  $[0^{\circ}/45^{\circ}/-45^{\circ}/90^{\circ}]$  with 32 plies for both spars and skins. The total thickness of all wing-box parts is t = 4mm. The quasi-isotropic-32/16 configuration reduces the number of plies in the rear spar. 16 plies in the rear spar

result in a thickness of t=1mm. Front spar and both skins maintain 32 plies and a thickness of t=4mm. The quasi-isotropic-32/8 configuration reduces the number of plies in the rear spar. 8 plies in the rear spar result in a thickness of t=1mm. Front spar and both skins maintain 32 plies and a thickness of t=4mm.

The shear-baseline introduces the second lay-up orientation. A  $[45^{\circ}/-45^{\circ}]$  lay-up characterizes the shear configurations. All skins and spars consist of 32 plies and have a total thickness of t=4mm. The shear-32/16 configuration reduces the number of plies in the rear spar. 16 plies in the rear spar result in a thickness of t=1mm. Front spar and both skins maintain 32 plies and a thickness of t=4mm. The shear-32/8 configuration reduces the number of plies in the rear spar. 8 plies in the rear spar result in a thickness of t=1mm. Front spar and both skins maintain 32 plies and a thickness of t=4mm.

Configuration	Wing-Box Parts			
Configuration	Front Spar, Top and Bottom Skin	Rear Spar		
Quasi-Isotropic-Baseline	$[0^{\circ}/45^{\circ}/-45^{\circ}/90^{\circ}]_{4S}$	$[0^{\circ}/45^{\circ}/-45^{\circ}/90^{\circ}]_{4S}$		
Quasi-Isotropic-32/16	$[0^{\circ}/45^{\circ}/-45^{\circ}/90^{\circ}]_{4S}$	$[0^{\circ}/45^{\circ}/-45^{\circ}/90^{\circ}]_{2S}$		
Quasi-Isotropic-32/8	$[0^{\circ}/45^{\circ}/-45^{\circ}/90^{\circ}]_{4S}$	$[0^{\circ}/45^{\circ}/-45^{\circ}/90^{\circ}]_{S}$		
Shear-Baseline	$[45^{\circ}/-45^{\circ}]_{8S}$	$[45^{\circ}/-45^{\circ}]_{8S}$		
Shear-32/16	$[45^{\circ}/-45^{\circ}]_{8S}$	$[45^\circ/-45^\circ]_{4S}$		
Shear-32/8 ´	$[45^{\circ}/-45^{\circ}]_{8S}$	$[45^{\circ}/-45^{\circ}]_{2S}$		

Table 2 – Lay-up of the six investigated configurations.

The numerical analysis investigates the torsion moment around the x-axis  $T_x$  and the rotation around the x-axis  $\theta_x$  for all six configurations undergoing the imposed wing-box rotation. The torsional stiffness  $\frac{GJ}{L}$  of the wing-box is determined for all six configurations. The torsional stiffness is defined in equation 1 as a relation between torsion moment T and rotation  $\theta$ . Pre- and postbuckling wing-box behavior is expected for the imposed wing-box deflection. Therefore, the buckling point of all six configurations is determined and the torsional stiffness is calculated for the pre- and postbuckling area of the deflection,  $\frac{GJ}{L}_{post}$  and  $\frac{GJ}{L}_{post}$ .

$$\frac{GJ}{L} = \frac{T}{\theta} \tag{1}$$

To compare the torsional stiffness before and after the buckling point, a reduced torsional stiffness  $\frac{GJ}{L}_{red}$  is introduced in equation 2. This reduced torsional stiffness describes the reduction of stiffness during the deflection as a relation between post- and prebuckling stiffness.

$$\frac{GJ}{L}_{red} = \frac{\frac{GJ}{L}_{post}}{\frac{GJ}{L}_{pre}} \tag{2}$$

# 3. Numerical Analysis

The finite-element model of the wing-box model is analyzed with the *ABAQUS* finite-element code. The model consists of a single layer of 4-node quadrilateral *S4R* shell elements. A mesh convergence study is performed to determine the mesh size. An element length of 10mm is selected combining best convergence and minimized calculation time.

The boundary conditions of the tip and root frame are modeled as simple displacement and rotation constraints. The root frame is constrained regarding displacement  $u_{x,y,z}$  along any axis and rotation  $\theta_{x,y,z}$  around any axis. The tip frame allows displacements  $u_{y,z}$  along y- and z-axis and rotations around the x-axis. The  $u_x$  displacement and the  $\theta_{y,z}$  rotation is constrained at the tip frame to enable a stable and convergent numerical model for the numerical analyses. Multi-Point-Constraint-Interactions

(MPC) characterize a stiffening of the simplified wing-box model. The MPC keeps the distance between a selected reference point and the surface equal during the calculation and are introduced at each segment.

The first numerical analysis is an eigenvalue analysis to obtain the critical point for each configuration under investigation, where buckling occurs. Two eigenvalue analyses are conducted for each configuration to determine the buckling torsion moment around the x-axis  $T_{x,b}$  and the buckling rotation around the x-axis  $\theta_{x,b}$ .

The second numerical analysis is a nonlinear dynamic implicit analysis to obtain the response of the wing-box for the imposed rotation. A rotation constraint  $\theta_x$  around the x-axis at the centerpoint of the tip frame applies the load as rotational displacement. The load application speed is  $\nu = 10 \frac{\circ}{s}$ . The dynamic implicit solver performs the calculations with a numerical damping factor  $\alpha = -0.33$  and the maximum time step is set to 0.05s. The implicit dynamic solver is chosen, because it is time efficient and as accurate as dynamic explicit and as nonlinear static.

## 4. Results

Table 3 presents the buckling rotation and the buckling moment calculated with the eigenvalue analysis.

The buckling moment and rotation drop about 80% for the quasi-isotropic-32/16 compared to the quasi-isotropic-baseline configuration. The comparison between quasi-isotropic-32/16 and quasi-isotropic-32/8 shows a 87% decrease in buckling moment and buckling rotation. The buckling moment drops 84% and the buckling rotation drops 77% for the shear-32/16 compared to the shear-baseline configuration. The comparison between shear-32/16 and shear-32/8 shows a 90% decrease in buckling moment and a 83% decrease in buckling rotation.

The quasi-isotropic-baseline has a similar buckling moment and a 42% higher buckling rotation than the shear-baseline. The quasi-isotropic-32/16 has a 16% higher buckling moment and a 33% buckling rotation than the shear-32/16. The quasi-isotropic-32/8 has a 35% higher buckling moment and a 14% buckling rotation than the shear-32/8.

Configuration	Buckling Rotation $\theta_{x,b}$	Buckling Moment $T_{x,b}$	
Comiguration	[°]	[kNm]	
Quasi-Isotropic-Baseline	5.33	105.92	
Quasi-Isotropic-32/16	1.06	19.93	
Quasi-Isotropic-32/8	0.14	2.62	
Shear-Baseline	3.08	103.41	
Shear-32/16	0.71	16.76	
Shear-32/8	0.12	1.69	

Table 3 – Buckling rotation and moment of the six investigated configurations.

Figure 2 shows the visualization of the buckling mode for the six investigated configurations with the eigenvalue analysis.

Figure 2a and 2b depicts the buckling mode of the shear- and quasi-isotropic baseline. For both configurations, the buckling deformation is visible on parts of the wing-box. For the configurations quasi-isotropic-32/16 (figure 2c) and quasi-isotropic-32/8 (figure 2e) as well as shear-32/16 (figure 2d) and shear-32/8 (figure 2f), the buckling only occurs on the rear spar. The buckling deformation and distribution along the rear spar varies for the six investigated configurations.

According to the eigenvalue analysis, a reduction in plies in the rear spar reduces constantly the buckling moment and buckling rotation as expected. A change in lay-up orientations produces a minor reduction in the buckling moment. However, a change in lay-up orientations shows a major influence on buckling rotation.

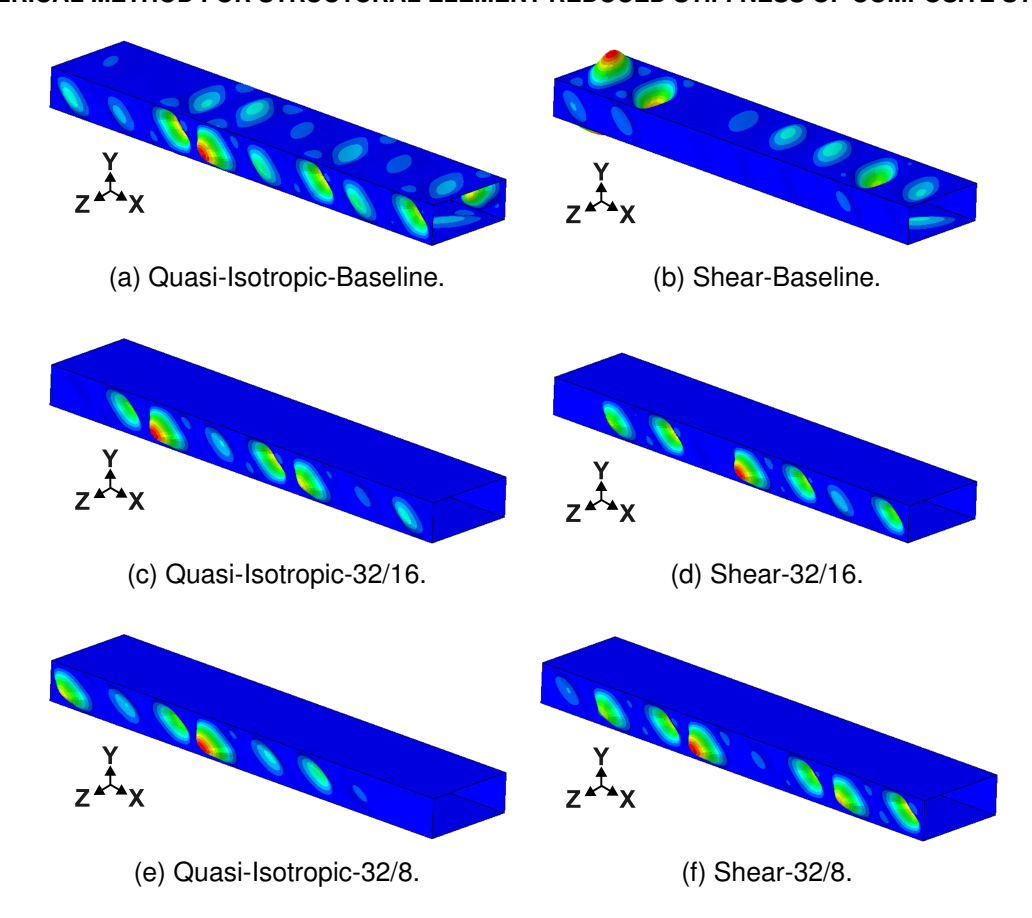


Figure 2 – Visualization of first buckling mode for all six investigated configurations.

Figure 3 shows the torsion moment in dependency of rotation for the six configurations calculated with nonlinear dynamic analysis.

The quasi-isotropic-baseline shows a linear behavior until reaching the buckling point. After the buckling point, the curve gradient decreases and the curve exhibits a nonlinear behavior.  $10^{\circ}$  rotation requires 175kNm torsion moment for the quasi-isotropic-baseline. The reduction in rear spar plies results in a lower gradient in the prebuckling linear and postbuckling nonlinear area for quasi-isotropic-32/16 compared to the quasi-isotropic-baseline. The required torsion moment for  $10^{\circ}$  rotation for quasi-isotropic-32/16 is reduced by 30% compared to the quasi-isotropic-baseline. The quasi-isotropic-32/8 torsion moment for  $10^{\circ}$  rotation is 33% less than for quasi-isotropic-32/16. The post-buckling gradient of the quasi-isotropic-32/8 curve is less compared with the quasi-isotropic-32/16 curve.

The shear-baseline shows a linear behavior until reaching the buckling point. After the buckling point, the curve gradient decreases and the curve exhibits a nonlinear behavior.  $10^{\circ}$  rotation requires 225kNm torsion moment for the shear-baseline. The reduction in rear spar plies results in a lower gradient in the prebuckling linear and postbuckling nonlinear area for shear-32/16 compared to the shear-baseline. The torsion moment for  $10^{\circ}$  rotation for shear-32/16 is reduced by 33% compared to the shear-baseline. The shear-32/8 torsion moment for  $10^{\circ}$  rotation is also 33% less than for shear-32/16. The postbuckling gradient of the shear-32/8 curve is comparable with the shear-32/8 curve.

The quasi-isotropic-baseline requires 22% less torsion moment for the required  $10^\circ$  rotation than the shear-baseline. The quasi-isotropic-32/16 and quasi-isotropic-32/8 need 20% less torsion moment for the required  $10^\circ$  rotation compared to shear-32/16 and shear-32/8. The prebuckling gradient of the shear-baseline, shear-32/16 and shear-32/8 curves is higher compared to the quasi-isotropic-baseline, quasi-isotropic-32/16 and quasi-isotropic-32/8 curves. Contrary to the prebuckling gradient, a significant difference in the postbuckling gradient is not experienced comparing shear curves with the quasi-isotropic curves.

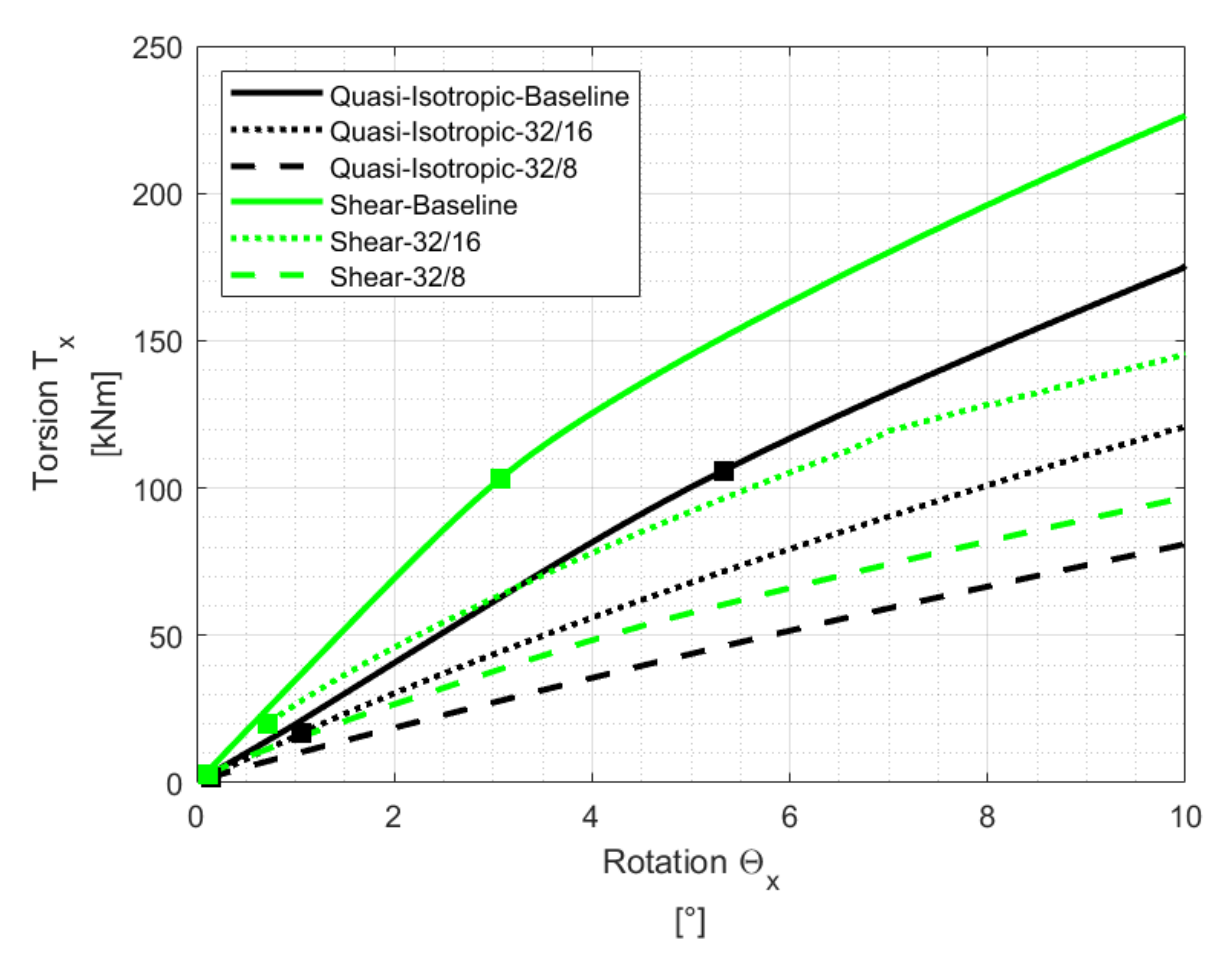


Figure 3 – Torsion-rotation curves for the six investigated configurations. Buckling points of six configurations are depicted as squares.

Table 4 presents the pre- and postbuckling torsional stiffnesses,  $\frac{GJ}{L\ pre}$  and  $\frac{GJ}{L\ post}$ , and the reduced torsional stiffnesses,  $\frac{GJ}{L\ red}$ , of the six configurations. The pre- and postbuckling torsional stiffnesses in the dynamic implicit analysis are determined in specific rotation regimes to ensure comparability. The rotation regimes have to avoid the vicinity of the buckling rotation for each configuration. Therefore, the prebuckling torsional stiffnesses are determined until reaching a rotation  $\theta_x=0.1^\circ$ . The rotation interval  $9^\circ < \theta_x < 10^\circ$  determines the postbuckling torsional stiffnesses.

The prebuckling torsional stiffness of quasi-isotropic-32/16 is 20% lower than the quasi-isotropic-baseline. The postbuckling torsional stiffness of quasi-isotropic-32/16 is 34% lower than the quasi-isotropic-baseline. The reduced torsional stiffness of quasi-isotropic-32/16 is 17% lower than the quasi-isotropic-baseline. A further reduction of rear spar plies results in a decrease of 33% for the prebuckling torsional stiffness and 24% for the postbuckling stiffness comparing quasi-isotropic-32/8 and quasi-isotropic-32/16. However, the reduced torsional stiffnesses for quasi-isotropic-32/8 and quasi-isotropic-32/16 are similar.

The prebuckling torsional stiffness of shear-32/16 is 20% lower than the quasi-isotropic-baseline. The postbuckling torsional stiffness of quasi-isotropic-32/16 is 33% lower than the shear-baseline. The reduced torsional stiffness of shear-32/16 is 17% lower than the shear-baseline. A further reduction of rear spar plies results in a decrease of 22% for the pre- and postbuckling torsional stiffness comparing shear-32/8 and shear-32/16. However, the reduced torsional stiffnesses for shear-32/8 and shear-32/16 are similar.

Comparing quasi-isotropic-baseline and shear-baseline, the postbuckling torsional stiffness shows a minor difference contrary to the prebuckling and reduced torsional stiffness. The prebuckling and reduced torsional stiffness are about 40% higher for shear-baseline than for quasi-isotropic-baseline.

A reduction in plies in the rear spar presents similar results for the comparison of quasi-isotropic-32/16 to shear-32/16. The prebuckling and reduced torsional stiffness are about 40% reduced for the quasi-isotropic-32/16 in comparison with shear-32/16. The postbuckling stiffnesses of quasi-isotropic-32/16 and shear-32/16 show a similar value. A further reduction in plies in the rear spar shows the same behavior for the comparison of quasi-isotropic-32/8 to shear-32/8. The prebuckling and reduced torsional stiffness are also about 40% smaller for the quasi-isotropic-32/8 in comparison with shear-32/8. The postbuckling stiffnesses of quasi-isotropic-32/8 and shear-32/8 show a minor difference.

Configuration	$\frac{GJ}{L}$ pre	$\frac{GJ}{L}$ post	$\frac{GJ}{L}$ red
c ogaau.o	$\left[\frac{kNm}{\circ}\right]$	$\left[\frac{kNm}{\circ}\right]$	[-]
Quasi-Isotropic-Baseline	1161.98	833.00	0.72
Quasi-Isotropic-32/16	922.55	551.70	0.60
Quasi-Isotropic-32/8	708.12	419.35	0.59
Shear-Baseline	1995.11	854.85	0.43
Shear-32/16	1600.44	570.76	0.36
Shear-32/8	1253.81	443.09	0.35

Table 4 – Pre- and postbuckling and reduced torsional stiffnesses for the six investigated configurations.

Figure 4 shows the  $u_y$ -displacement into the y-direction after  $\theta_x = 10^\circ$  rotation around the x-axis for the six investigated configurations for the dynamic implicit analysis results.

Quasi-isotropic-baseline (figure 4a) presents an upward deflection of the front spar and downward deflection of the rear spar of similar magnitude around the x-axis of the wing-box. Quasi-isotropic-32/16 shows a different deformation (figure 4c) than the quasi-isotropic-baseline. The magnitude of the downward deflection of the rear spar is higher than the downward deflection for quasi-isotropic-baseline. Contrary, the upward deflection of the front spar has a lower magnitude than quasi-isotropic-baseline. Hence, the magnitude of the downward deflection of the rear spar is higher than the magnitude of the upward deflection of the front spar for the quasi-isotropic-32/16 configuration. Quasi-isotropic-32/8 (figure 4e) shows a similar deflection behavior as quasi-isotropic-32/16. The magnitude of the downward deflection of the rear spar is higher for quasi-isotropic-32/8 than quasi-isotropic-32/16.

Shear-baseline (figure 4b) presents an upward deflection of the front spar and downward deflection of the rear spar of similar magnitude around the x-axis of the wing-box. Shear-32/16 shows a different deformation (figure 4d) than the shear-baseline. The magnitude of the downward deflection of the rear spar is higher than the downward deflection for shear-baseline. Contrary, the upward deflection of the front spar has a lower magnitude than shear-baseline. Hence, the magnitude of the downward deflection of the rear spar is higher than the magnitude of the upward deflection of the front spar for the shear-32/16 configuration. Shear-32/8 (figure 4f) shows a similar deflection behavior as shear-32/16. The magnitude of the downward deflection of the rear spar is higher for shear-32/8 than shear-32/16.

The comparison of the quasi-isotropic-baseline configuration with the shear-baseline configuration shows no differences in the deflection behavior or magnitude. Quasi-isotropic-32/16 and shear-32/16 as well as quasi-isotropic-32/8 and shear-32/8 also have presents a similar deflection behavior and magnitude.

According to the dynamic implicit analysis, the results show a significant influence of the lay-up orientation of the rear spar on the reduced torsional stiffness and prebuckling torsional stiffness. Contrary, the postbuckling torsional stiffness is significantly influenced by a reduction of the number of plies of the rear spar and not by the lay-up orientation. The reduced torsional stiffness stays for wing-boxes, with a reduction in the number of plies of the rear spar, the same, if the number of plies of the rear spar is lower than the number of plies in the other wing-box parts. The higher torsion moment for the

required rotation for the shear configuration is caused by the higher prebuckling stiffness of the shear configurations compared to their respective quasi-isotropic configurations. The rotation deformation changes shape with a reduction of plies in the rear spar. The rotation gets asymmetrical around the x-axis and the rear spar is exposed to a higher downward deflection magnitude.

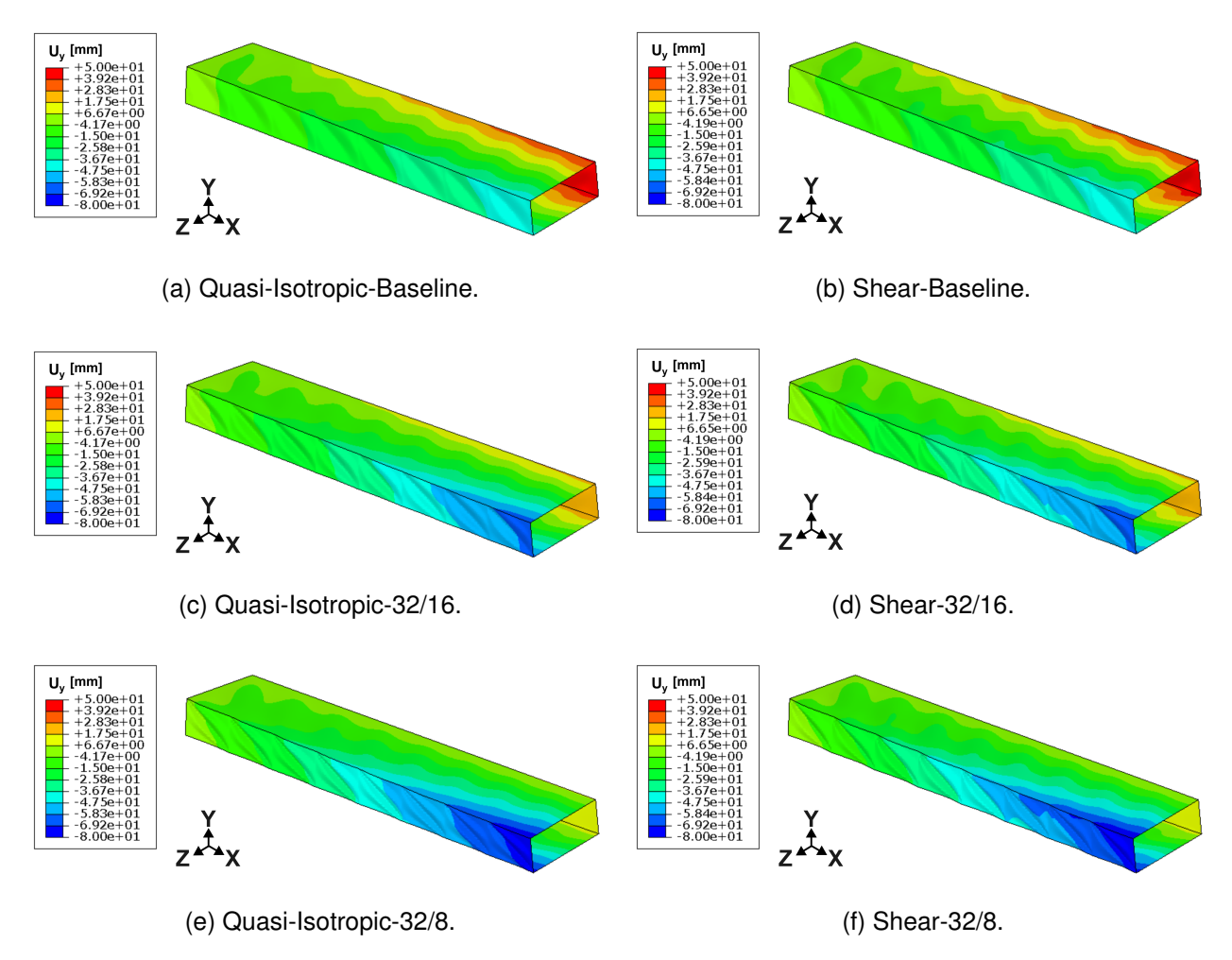


Figure 4 –  $u_v$ -displacement for the six investigated configurations for  $\theta_x = 10^\circ$ .

## 5. Conclusion

In this paper, a numerical analysis of a composite wing-box experiencing torsion is presented. The analysis investigates the influences of two different lay-up orientations and three different numbers of plies for the rear spar on the pre- and postbuckling torsional stiffness.

Eigenvalue analysis determines the buckling moment and buckling rotation of the wing-box for the six different configurations. The dynamic implicit analysis presents the torsion-rotation curves and preand postbuckling torsional stiffness as well as reduced torsional stiffnesses introduced as a relation between pre- and postbuckling.

Eigenvalue analysis shows, that a reduction in ply number for the rear spar results in decreased buckling rotation and moment as expected, whereas the lay-up orientation only significantly influences the buckling rotation. The dynamic implicit analysis shows, that prebuckling and reduced torsional stiffness have a strong dependency on the lay-up orientation within the rear spar. A change in lay-up orientation leads to higher moments for desired wing-box rotations due to higher prebuckling torsional stiffness. The deformation distribution of the wing-box is influenced by the reduction of the number of plies in the rear spar. This reduction leads to an asymmetrical rotation and a higher downward deflection of the rear spar compared to the front spar as expected.

In the next step, the material failure will also be investigated for the wing-box under torsion as well as a more detailed and realistic wing-box structure.

### 6. Outlook

The next generation of aircraft needs lighter and more adaptive structures to meet the targets for decreasing emissions. Passively morphing aerospace structures are an opportunity to fulfill the requirements.

This numerical study is conducted as the first step of a methodology to conceive how to design passively adaptive aerospace structures. In this approach, the desired shapes of a structure are defined first. These desired shapes are then transferred onto local elements of the structure, where the buckled shape is obtained using the reduced stiffness.

This new methodology will be applied for the design of a wing-box and validated by static and wind tunnel tests.

## 7. Acknowledgments

Funded by the European Union (ERC Advanced Grant, NABUCCO, project number 101053309). Views and opinions expressed are, however, those of the author only and do not necessarily reflect those of the European Union or the European Research Council Executive Agency. Neither the European Union nor the granting authority can be held responsible for them.







## 8. Contact Author Email Address

Sebastian Stammel - sebastian.stammel@polimi.it Chiara Bisagni - chiara.bisagni@polimi.it

# 9. Copyright Statement

The authors confirm that they, and/or their company or organization, hold copyright on all of the original material included in this paper. The authors also confirm that they have obtained permission from the copyright holder of any third-party material included in this paper to publish it as part of their paper. The authors confirm that they give permission, or have obtained permission from the copyright holder of this paper, for the publication and distribution of this paper as part of the ICAS proceedings or as individual off-prints from the proceedings.

## References

- [1] Weisshaar T. Morphing aircraft systems: Historical perspectives and future challenges. *Journal of Aircraft*, Vol. 50, No.2, pp 337-353, 2013.
- [2] Wagg D, Bond I, Weaver P, and Friswell M. *Adaptive Structures: Engineering Applications*. John Wiley & Sons, 2007.
- [3] Garcia H, Abdulrahim M, and Lind R. Roll control for a micro air vehicle using active wing morphing. *AlAA Guidance, Navigation, and Control Conference and Exhibit*, Austin, 2003.
- [4] Rivas J, Boston D, Boddapati K, and Arrieta A F. Aero-structural optimization and actuation analysis of a morphing wing section with embedded selectively stiff bistable elements. *Journal of Composite Materials*, Vol. 57, No.4, pp 737-757, 2023.
- [5] Bisagni C and Sala G. Buckling and shape control of composite laminates using embedded shape memory alloys wires. *45th AIAA/ASME/ASCE/AHS/ASC Structures, Structural Dynamics & Materials Conference*, Palm Springs, 2004.
- [6] Airoldi A, Crespi M, Quaranti G, and Sala G. Design of a morphing airfoil with composite chiral structure. *Journal of Aircraft*, Vol. 49, No. 4, pp 1008-1019, 2012.
- [7] Arrieta A F, Kuder I, Rist M, Waeber T, and Ermanni P. Passive load alleviation aerofoil concept with variable stiffness multi-stable composites. *Composite Structures*, Vol. 116, pp 235-242, 2014.
- [8] Reis P. A perspective on the revival of structural (in) stability with novel opportunities for function: From buckliphobia to buckliphilia. *Journal of Applied Mechanics*, Vol. 82, No. 11, pp 111001, 2015.

- [9] Zhang J and Bisagni C. Buckling-driven mechanisms for twisting control in adaptive composite wings. *Aerospace Science and Technology*, Vol. 118, pp 107006, 2021.
- [10] Dávila C and Bisagni C. Fatigue life and damage tolerance of postbuckled composite stiffened structures with initial delamination. *Composite Structures*, Vol. 161, pp 73-84, 2016.
- [11] Cordisco P and Bisagni C. Cyclic buckling tests under combined compression and shear on composite stiffened panels. *AIAA Journal*, Vol. 47, No. 12, pp 2879-2893, 2009.
- [12] Yan Z, Zhang F, Wang J, Liu F, Guo X, Nan K, Lin Q, Gao M, Xiao D, Shi Y, Qiu Y, Luan H, Kim J, Wang Y, Luo H, Han M, Huang Y, Zhang Y, and Rogers J. Controlled mechanical buckling for origami-inspired construction of 3d microstructures in advanced materials. *Advanced Functional Materials*, Vol. 26, No. 16, pp 2585-2769, 2016.
- [13] Potter K and Weaver P. A concept for the generation of out-of-plane distortion from tailored frp laminates. *Composites Part A: Applied Science and Manufacturing*, Vol. 35, No. 12, pp 1353-1361, 2004.
- [14] Cui Y and Santer M. Characterization of tessellated bistable composite laminates. *Composite Structures*, Vol. 137, pp 93-104, 2015.
- [15] Dassault Systems. Abaqus analysis guide. 2024.
- [16] Bisagni C, Vescovini R, and Davila C G. Single-stringer compression specimen for the assessment of damage tolerance of postbuckled structures. *Journal of Aircraft*, Vol. 48, No. 2, pp 492-502, 2007.